Analysis of the two-point wheel-rail contact scenario using the knife-edge-equivalent contact constraint method

Javier F. Aceituno[a,*], Pedro Urda[b], Eduardo Briales[c], José L. Escalona[b]

[a] *Departamento de Ingeniería Mecánica y Minera. Universidad de Jaén, Spain*
[b] *Departamento de Ingeniería Mecánica y Fabricación. Universidad de Sevilla, Spain*
[c] *Virtualmechanics, S.L. Sevilla, Spain*

Abstract

This paper presents a rigid contact approach to analyse the two-point wheel-rail contact scenario using the simplified constraint-based contact method called *Knife-edge Equivalent Contact method* (KEC-method). The proposed approach makes use of the computationally efficient online solution of the KEC constraints, where a single-point rail is in contact with an equivalent wheel profile, and provides an exact relation between the location of the contact points in the equivalent and real profiles. In this context, the two-point contact scenario can be easily dealt by linearly softening the KEC-constraints in the vicinity of the two-point contact, that gives a continuous and unique contact point solution between each wheel-rail pair and avoids finite contact point jumps between tread and flange. This allows an efficient kinematic solution of the two-point contact scenario. However, to properly account for a dynamic equivalence of the two-point contact scenario in the computation of the tangential contact forces, the reaction force acting on the wheel when the contact point lies on the tread-flange transition, is transformed into two contact forces acting on the tread and flange respectively maintaining the resultant equilibrium of forces at the wheel.

Keywords: Wheel-rail contact, Two-point contact scenario, KEC-method, Online constraint contact approach

1. Introduction

The modelling of the wheel-rail contact is essential in the multibody simulation of railway vehicles. Generally, wheel and rail profile surfaces in contact result in non-conformal contacts between wheel tread and rail. However, there are situations (i.e. contact at root of the wheel or contact of heavily worn wheel-rail profiles), in which conformal or quasi-conformal contacts may occur that lead to computationally demanding evaluations of the location of the contact points. These locations are crucial for an accurate estimation of the normal and tangential contact forces, which are the responsible of the dynamic behaviour of a railway vehicle [1]. In this context, efficient and precise models that deal with this geometric issue are of great interest for the research community.

In the literature, there are two well-known and classical approaches to model the wheel-rail contact in multibody simulations of railway vehicles [2]; (a) the elastic approach, where an interpenetration of the undeformed surfaces of wheel and rail is admissible, and (b) the constraint approach, where no interpenetration of the undeformed surfaces is admissible so that the surfaces coincide in one or more singular contact points.

The elastic approach [3], which is used in general vehicles dynamics more often than the rigid one, has the capability of directly dealing with many railway situation scenarios in which wheel separation may occur, such as wheel climb, derailment or two-point wheel-rail contact. In general, many research works

*Corresponding author
Email addresses: jaceitun@ujaen.es (Javier F. Aceituno), purda@us.es (Pedro Urda), e.briales@virtualmech.com (Eduardo Briales), escalona@us.es (José L. Escalona)

can be found using this contact approach. In the work of Magalhães et al. [4], an elastic contact model for non-Hertzian conditions is proposed and compared to Hertzian methods leading to accurate results and fast simulations. In Pombo et al. [5], a three-dimensional elastic online detection method that can evaluate two-point contact scenarios and lead and lag flange contacts (longitudinally displaced contacts due to high values of wheelset yaw angle), is proposed and also evaluated in [6]. This work has been the subject of further investigations for the inclusion of track irregularities [7] and more recently for the inclusion of track flexibility in the online contact detection [8]. Another elastic approach can be found in the work of Malvezzi et al. [9], where two contact elastic detection methods are proposed based on analytical expressions of the wheel and rail surfaces. Both methods are reduced to a single one-scalar equation of one unknown variable giving efficient computational times and accurate contact points locations as shown in [10]. Also, Baeza et al. [11] propose an elastic approach to determine interpenetration areas between wheel and rail surfaces allowing three dimensional displacements of the wheelset. Notwithstanding, the use of an elastic wheel-rail contact approach has a great disadvantage: the force element representing the wheel-rail contact has a high normal contact stiffness compared to the stiffnesses of the suspension elements. As a result, the equations of motion form a system of stiff differential equations. The solution of stiff differential equations requires the use of implicit integrators with very small time steps, what leads to high computational times.

In the rigid contact approach or constraint approach, no indentation or separation of the wheel and the rail occurs. Therefore, the introduction of the high contact stiffness into the equations of motion is avoided so that the solution of the equations is more computationally efficient. In this context, the work of Muñoz et al. [12] presents a multibody model of railway vehicles that uses simplified contact constraints for the wheel tread combined with an elastic approach for the flange. The use of exact or simplified constraints may involve different number of constraints and surface parameters, but as presented by Escalona et al. [13], they all reduce the same number of wheelset relative track degrees of freedom (DOFs): one per wheel-rail pair. This way, contact solution can be obtained by a set of minimum independent variables, which leads to the possibility to precompute the contact solution and use it as an offline search method known as contact lookup table. In [14], a formulation that employs rigid wheel-rail contact lookup tables that accounts for track irregularities by means of two independent variables (2-DOFs) is proposed and compared with the online solution of the contact constraints. This work shows that, analysing carefully with the geometric assumptions, contact lookup tables can provide efficient and precise results. Other applications of contact lookup tables can be found in [15, 16, 17, 18, 19]. In Santamaría et al. [15], an elastic approach to obtained a reduced 3-DOFs contact table is presented. In the work of Sugiyama et al. [16] a constraint contact lookup table approach is derived for the wheel tread contact while for the flange one, an elastic online search is performed. This work avoids the problems associated with the use of a rigid contact approach when flange contact occurs: the finite contact point jump. In addition, in [17], the contact problem in turnouts is analysed by multiple contact lookup tables based on a combined nodal search of the wheel and rail surfaces to determine significant contact point jumps and a non-conformal contact geometry approach to determine their exact locations. More recently, Piotrowski et al. [18] describe the regularization of the non-elliptical wheel-rail contact patches for a fast computation of creep forces named Kalker book of tables for non-Hertzian contact (KBTNH). This approach has been used in current works as in [19] for the analysis of size and accuracy of contact lookup tables and in [20] for the computation of the wheel-rail contact patch moments.

In general, although most of the wheel-rail contact models used for railway vehicle models are based on elastic approaches, the use of constraint contacts for this application is a precise and effective method. However, when flange contact occurs (i.e. at sharp curves, turnouts or derailment), contact point jumps imply numerical instabilities at contact constraints. In this context, the so-called *quasi-elastic* wheel-rail contact method was introduced in [21, 22]. The quasi-elastic contact method considers the elastic deformation of the contact surfaces and weights contact constraints to avoid contact point jumps, leading to a continuous transition from tread to flange contact and reducing computational cost. Although this method does not reproduce wheel climb scenarios, it has been widely used and implemented in commercial simulation packages such as Simpack [23].

In the goal of avoiding numerical instabilities associated with constraint contact and contact point jumps, Escalona et al. [13] presents a simplified constraint approach called *Knife-edge Equivalent Contact*-method

(KEC-method). The KEC-method is based on a classical approach used in mechanics, where a wheel contacts a single point rail. However, the wheel profile is an equivalent wheel profile because it is defined such that it produces the same wheelset relative motion with respect to the track that using real wheel-rail profiles (see Fig. 3). In this sense, the contact between a wheel profile and a single point rail gives a continuous solution of the contact point from tread to flange. This fact eliminates the continuity problems of the constraints in double contact point scenarios. Nonetheless, the values of the normal contact forces at each of the two contact points are not determined.

For this reason, the goal of this work is to present an approach based on the rigid contact KEC-method to deal online and efficiently with the two-point contact scenario. To this end, the correspondence between the locations of the contact points in the equivalent and real profiles is first determined to then soften the contact constraints in the vicinity of the two-point scenario. This way, contact forces are obtained smoothly between tread and flange in an efficient computational manner. Then, to appropriately account for contact forces, smoothed solutions between tread and flange are translated to realistic tread and flange locations. This results in an online and computationally simple constraint contact approach that can deal with the wheel-rail contact in many simulation scenarios.

The paper is organized as follows: Section 2 explains the drawbacks associated with contact constraints in two-point wheel-rail contact scenarios. In Sect. 3, the principles of the KEC-method are detailed together with Sect. 4, which shows how this method originally deals with wheel-rail contact forces. In Sect. 5, the application of the KEC-method to account for the two-point wheel-rail contact scenario is presented. Then, Sect. 6 briefly introduces the compact form of the equations of motion and Sect. 7 provides simulation results of two different case studies in which clear two-point contact scenarios occur: a single unsuspended wheelset and a bogie vehicle negotiating ideal tracks formed by a tangent, a transition and a constant curve segments. Finally, Sect. 8 provides some conclusions and summary.

2. Why the contact constraint method is not suited to simulate two-point contact scenario

The wheel-rail contact can be modelled as a *surface-to-surface* non-conformal contact constraint. The wheel profile can be modelled as a solid of revolution. The rail-head profile can be modelled as an extruded solid. Both surfaces can be parametrically described using two surface parameters: the transverse parameter s_1^{rw} and the angular parameter s_2^{rw} for the wheel, and the longitudinal parameter s_1^{rr} and the transverse parameter s_2^{rr} for the rail, see Fig. 1. Each wheel rail contact is modelled using five constraints: 3 contact position constraints (contact point in the wheel and rail are located in the same position) and 2 orientation constraints (tangent plane to the wheel at the contact point parallel to the tangent plane to the rail at the contact point). These 5 constraints are algebraic equations written in terms of the 6 generalized coordinates of the wheel (3 translational coordinates, 3 orientation coordinates) and 4 surface parameters (2 for the wheel, 2 for the rail). Because a wheelset has two wheels in contact with two rails, the total number of constraints is 10 and the total number of surface parameters is 8. The wheel-rail contact eliminates 2 relative degrees of freedom of the wheelset motion, as follows:

$$g = n_q + n_s - m = 6 + 8 - 10 = 4 \tag{1}$$

where g is the number of wheelset degrees of freedom, n_q is the number of generalized coordinates, n_s is the number of surface parameters, and m is the number of constraints.

The situation described above occurs in railway applications in the most common case in which the wheels contact the railheads in the treads. For some wheel and rail profile combinations, when the lateral displacement of the wheelset is large enough, sudden flange contact occurs, reaching the situation shown in Fig. 2. In this case, three wheel-rail contacts occur: on the left tread (LT in the figure), on the right tread (RT in the figure) and on the right flange (RF in the figure). In the new situation, the wheelset would have three degrees of freedom (five added constraints, four added surface parameters), as follows:

$$g = n_q + n_s - m = 6 + 12 - 15 = 3 \tag{2}$$

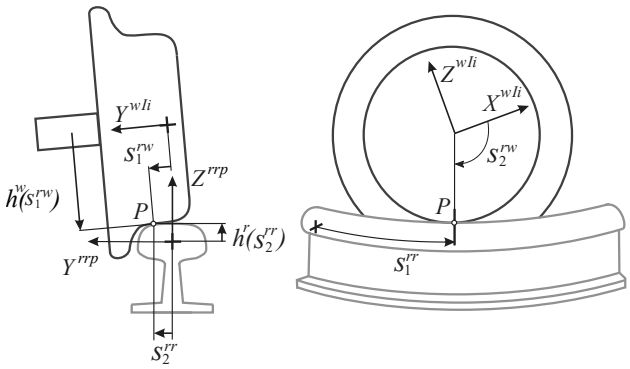

Figure 1: Wheel-rail contact geometry

Clearly, there is a change in the kinematic structure of the system (number of kinematic constraints and number of degrees of freedom). In general, the flange contact occurs with non-zero relative velocity of approach of the wheel and rail surfaces at the contact point, this is, under impact conditions. That means that, at the exact instant when the surfaces touches the flange, the contact constraints are fulfilled at position level, but not at velocity level. As a consequence, time-integration has to be stopped and the generalized impulse-momentum balance equations [24] have to be solved to find the required velocity jumps in the generalized coordinates to continue the simulation. The generalized impulse-momentum balance equations include as an input the value of the coefficient of restitution. Assuming a zero value of the coefficient of restitution means that the flange contact constraint will persist for a while (as it occurs frequently in reality), while assuming a value between zero and one results in an instantaneous contact. Clearly, when deciding the value of the coefficient of restitution, the analyst intervenes in the simulation so that the result is practically arbitrary. If flange contact persists (a zero coefficient of restitution is selected), in the subsequent period, the Lagrange multipliers associated with the flange contact have to be monitored to check possible *pulling* normal contact forces. Under these conditions, the flange contact constraints have to be removed, thus changing again the kinematic structure of the system. In summary, addition-deletion of flange contact constraints to analyse 2 point-contact scenario is cumbersome, difficult to program and may produce arbitrary results.

Because of the problem of determining the normal contact forces for two contact points in one wheel-rail contact, the description of simultaneous contact at the tread and at the flange is simply unfeasible. Instead, an elastic method is used for flange contact, leading to the so-called hybrid method [3] if the tread contact is modelled with constraints. However, the elastic flange contact requires significant reduction in the value of the integration time-step when flange contact occurs and the simulation outputs depend excessively in the assumed contact stiffness.

The method described in next sections can be used to model both tread and flange contact with constraints, avoiding the difficulties described in the previous paragraphs. This method leads to smoothed simulations, without sudden changes in the kinematic structure of the the system and without velocity jumps in the system coordinates, when modelling two-point contact scenarios.

3. Description of the KEC-method

This section summarises the principles, constraints and wheel-rail profile combination of the knife-edge equivalent contact method for its use in multibody simulations of railway vehicles [13].

3.1. Basis of the KEC-method

As introduced, the KEC-method is a rigid or constraint-based simplified contact method that assumes permanent contact between the running surfaces of wheel and rail without indentation or separation of the

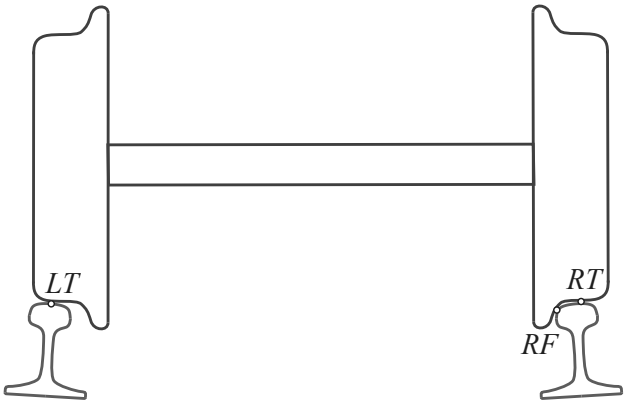

Figure 2: Two-point contact scenario

surfaces. Therefore, it is not a method that evaluates the inner details of contact mechanics such as contact patch, sliding and sticking areas or pressure distribution.

In this sense, as other classical rigid contact approaches [13], each wheel-rail contact using KEC constraints eliminates one wheelset-track relative degree of freedom. The wheel-rail contact problem can be simplified from a spatial *surface-to-surface* contact problem, as described in Sect. 2 and from now on called *exact contact constraints*, to a planar *curve-to-curve* contact problem. This is an accurate approximation that produces accurate results in most railway dynamics simulations [14]. These constraints will be called *approximate contact constraints*. In the approximate contact constraints, it is considered that the wheelset yaw angle is zero, $\psi^{wi} = 0$, and this value is substituted in the exact contact constraints. As a consequence, two simplifications arise: (a) that the longitudinal parameters of the contact points on the rails coincide with the longitudinal position of the wheelset along the track s^{wi} and (b) the angular parameters of the contact points on the wheels are all 90°, because they lie in the YZ plane of the wheelset-track frame, wti, see Fig. 3. That way, the railhead curve and the wheel profile curve where the contact points are located are defined. Therefore, the reduction to the planar problem implies that only transverse parameters on the wheel and rail (2 parameters instead of 4 per contact) are needed to fully locate the contact points; this is, 1 parameter per curve profile. Thus, the simplifications on the contact constraints exploit the fact that the rail is an extruded body and the wheel is a solid of revolution. Without these properties, the assumed simplifications in the contact constraints would not be possible.

The approximate contact constraints are formulated by 3 equations required for the planar contact problem instead of 5 equations required for the spatial contact problem. Two equations represent the condition that in the contact point the two curves must have the same lateral and vertical positions. The third equation represents the condition that in the contact point the two curves must have the same slope or gradient; this can be formulated by the condition that the scalar product of the normal vector of one curve and the tangential vector of the other one must be zero. The number of degrees of freedom of the wheelset with two wheels in contact with the rails is, obviously, also 2, as follows:

$$g = n_q + n_s - m = 6 + 4 - 6 = 4 \tag{3}$$

The simulation of a railway vehicle using contact constraints requires to include in the equations of motion the surface parameters associated with the contact points as a set of non-generalized coordinates $\mathbf{s}$. The set $\mathbf{s}$ enters the equations of motion and it has to be integrated forward in time as it is the set of generalized coordinates $\mathbf{q}$. There is a method to eliminate the surface parameters of the equations of motion [25], however, the required calculations are so complex that this method is seldom used in practice. A very common alternative that also excludes $\mathbf{s}$ from the equations of motion is the use of *contact lookup tables* (CLT). CLT are obtained as the result of solving the contact constraints in a pre-process phase. When using the exact contact constraints, the equations have to be solved for a physically reasonable range of values of

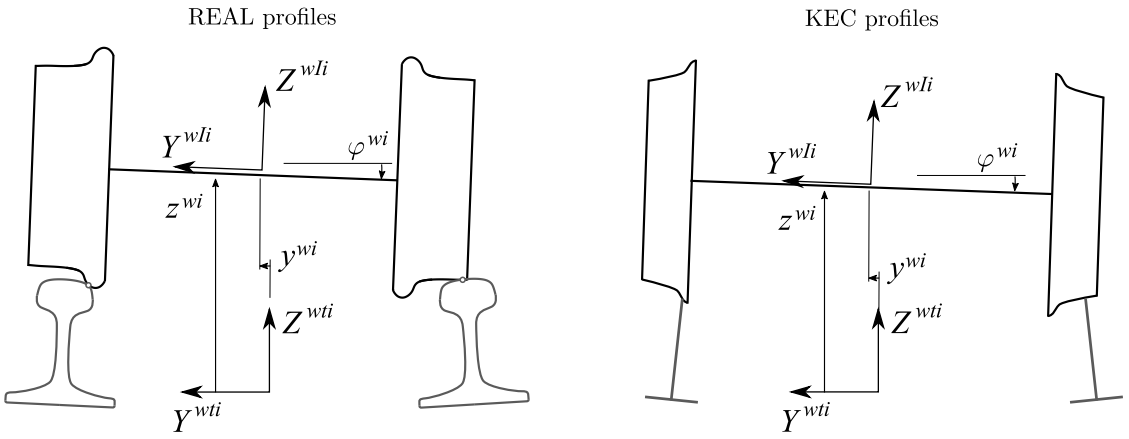

Figure 3: Wheelset kinematics using real and KEC profiles

the lateral displacement and yaw angle of the wheelset. When using the approximate contact constraints (influence of the yaw angle in the contact geometry is neglected), only the lateral displacement has to be varied in the given range. In the paper [14], the use of CLT with the latter option is described. Entering the CLT with the lateral displacement of the wheelset y^{wi} provides the value of the vertical displacement of the wheelset z^{wi}, the roll angle of the wheelset φ^{wi} and all required information about the contact geometry (i.e. location of the contact points, tangent and normal vectors or curvatures). The information stored in the CLT can be interpreted, in part, as tabulated functions of the form:

$$z^{wi} = z^{clt}\left(y^{wi}\right), \quad \varphi^{wi} = \varphi^{clt}\left(y^{wi}\right), \tag{4}$$

Figure 4 shows the plot of these functions for the wheel and rail profiles used in [13]. The use of CLT is equivalent to say that, out of the 6 generalized coordinates of the wheelset, 4 are independent and 2 are dependent, as follows:

$$\begin{aligned} \mathbf{q}^{wi} &= \left[\begin{array}{cccccc} s^{wi} & y^{wi} & z^{wi} & \varphi^{wi} & \theta^{wi} & \psi^{wi} \end{array}\right]^T, \\ \mathbf{q}^{wi}_{ind} &= \left[\begin{array}{cccc} s^{wi} & y^{wi} & \theta^{wi} & \psi^{wi} \end{array}\right]^T, \\ \mathbf{q}^{wi}_{dep} &= \left[\begin{array}{cc} z^{wi} & \varphi^{wi} \end{array}\right]^T \end{aligned} \tag{5}$$

Clearly, the tabulated functions given in Eq. 4 define the *subspace of allowable motion* associated with the set of coordinates $\mathbf{q}^{wi}$. Also note that, based on the approximate contact constraints, the independent coordinates θ^{wi} and ψ^{wi} are not relevant for the kinematic relations.

In the KEC-method it is assumed that the wheels contact rails that are just a line, infinitely narrow. The KEC-method finds the profile of the wheels such that the subspace of allowable motion of the wheelset is the same than the subspace defined by Eq. 4, as sketched in Fig. 3. With this method, the wheel-rail contact is further simplified to a *curve-to-point* contact problem. If the rails have zero width, the contact point on the rail is completely defined once the track cross-section is identified, without needing a transverse surface parameter on the rail. In addition, the contact constraints reduce to contact point constraints. Tangent plane constraints are not needed, simply because the tangent to a single point is not defined. The number of degrees of freedom of the wheelset with two wheels in contact with two rails defined with the KEC-method is given by:

$$g = n_q + n_s - m = 6 + 2 - 4 = 4 \tag{6}$$

Table 1 shows the reduction in the number of contact constraints and surface parameters when using exact contact constraints, approximate contact constraints and KEC-method.

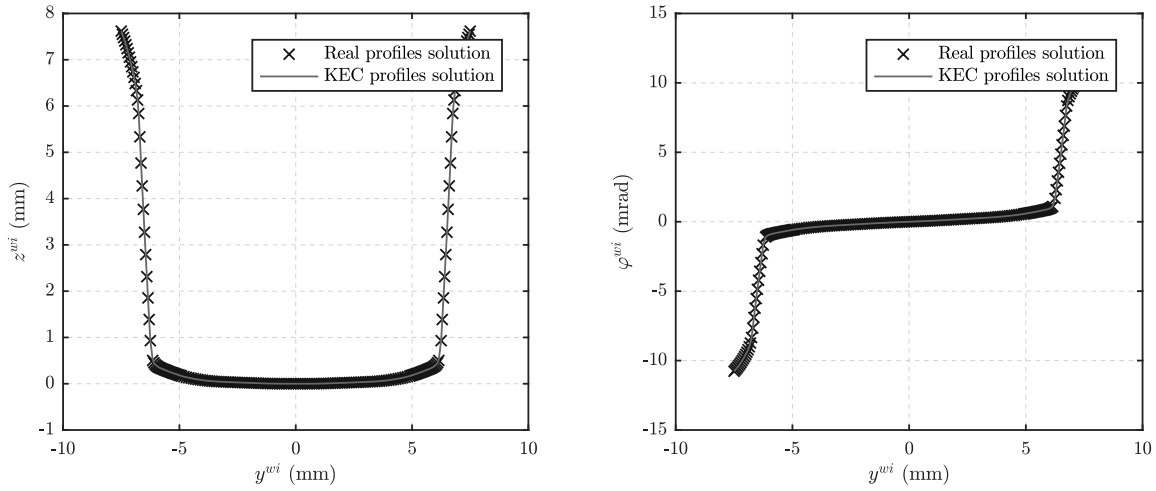

Figure 4: Wheelset kinematics (vertical z^{wi} and roll angle φ^{wi}) using real and equivalent profiles

Table 1: Types of contact constraints

Form	**# of C**	**# of s**
Exact (surface to surface)	10	8
Approximate (curve to curve)	6	4
KEC-method (curve to point)	4	2

3.2. KEC constraints

The geometric assumptions of the KEC-method can be seen in Fig. 5 that shows a wheelset in contact with an irregular track whose railhead cross-sections are assumed as single points (circles in the figure). In Fig. 5, the frame $< Y^{wti}, Z^{wti} >$ refers to the so-called *wheelset-track frame* of wheelset i. It is a frame that follows the wheelset movement keeping its $X-$axis tangent to the track centreline. Also, $< Y^{wIi}, Z^{wIi} >$ refers to the *wheelset-intermediate frame* [14], a frame that rigidly moves with the wheelset but shows no pitch rotation. Other variables shown in Fig. 5 can be listed as:

- L^r is the track half-gauge.
- L^w is the lateral local position of the wheel profile.
- r_0 is the rolling radius of the wheel when centred in a track with no irregularity.
- s^{lk} and s^{rk} are the transverse parameters of the contact point on the left and right equivalent wheel profile.
- z^{lir}, z^{rir}, y^{lir} and y^{rir} are the vertical and lateral irregularities of the left and right rails respectively.
- y^{wi}, z^{wi} and φ^{wi} are the relative degrees of freedom (lateral, vertical and roll angle) of the wheelset intermediate frame i with respect to the wheelset-track frame.
- $\mathbf{u}_{lc}^{wi}$ and $\mathbf{u}_{rc}^{wi}$ are the left and right contact points local position vectors with respect to the wheelset-intermediate frame.

The contact-point constraint equations of the wheelset shown in Fig. 5 can be written as:

$$\begin{aligned} \bar{\mathbf{r}}_{lc}^{wi}\left(\mathbf{q}^{wi}, s^{lk}\right) - \bar{\mathbf{r}}^{lir} &= \mathbf{0} \\ \bar{\mathbf{r}}_{rc}^{wi}\left(\mathbf{q}^{wi}, s^{rk}\right) - \bar{\mathbf{r}}^{rir} &= \mathbf{0} \end{aligned} \tag{7}$$

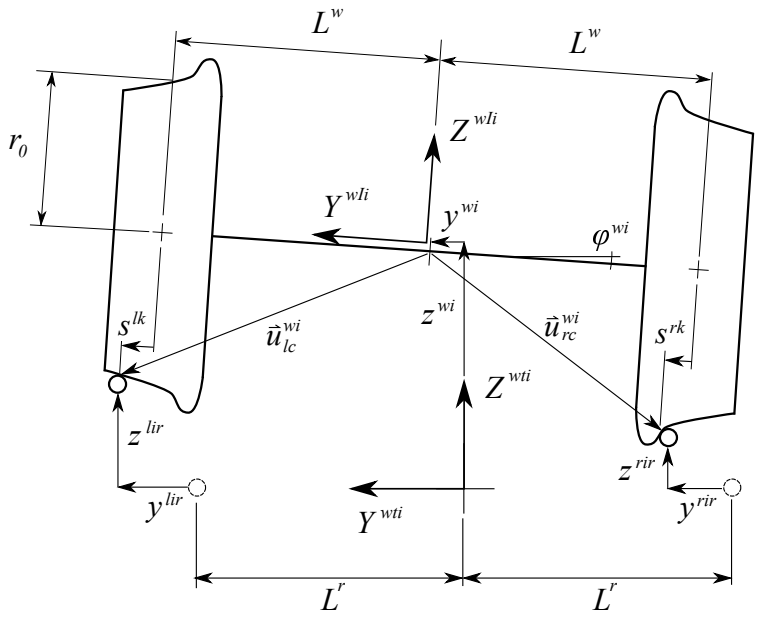

Figure 5: Wheelset with knife edge constraints

where $\bar{\mathbf{r}}^{lir}$ and $\bar{\mathbf{r}}^{rir}$ are the position-vectors of the left and right rails, and $\bar{\mathbf{r}}^{wi}_{lc}$ and $\bar{\mathbf{r}}^{wi}_{rc}$ are the position vectors of the contact points on the left and right wheels, respectively. Note that overline '*bar*' means that the components of these vectors are referred to the wheelset-track frame of Fig. 5. Also, terms in round brackets mean functional dependency.

With the assumption that the contact points lie in the vertical YZ plane of the wheelset-track frame and because the rails are supposed to have no width ($L^w = L^r$), Eq. 7 can be written as a system of the following four non-linear algebraic equations (two per wheel-rail pair):

$$\begin{aligned} y^{wi} + s^{lk} + \varphi^{wi}\left[r_0 + f^{lk}\left(s^{lk}\right)\right] - y^{lir} &= 0 \\ z^{wi} + \varphi^{wi}\left[L^w + s^{lk}\right] - f^{lk}\left(s^{lk}\right) - r_0 - z^{lir} &= 0 \\ y^{wi} + s^{rk} + \varphi^{wi}\left[r_0 + f^{rk}(s^{rk})\right] - y^{rir} &= 0 \\ z^{wi} + \varphi^{wi}\left[-L^w + s^{rk}\right] - f^{rk}\left(s^{rk}\right) - r_0 - z^{rir} &= 0 \end{aligned} \tag{8}$$

where as shown in Fig. 6 for the equivalent right wheel, the terms f^{lk} and f^{rk} are the functions that define the equivalent wheel profile evaluated at the parameters s^{lk} and s^{rk} respectively. Note that the roll angle is linearised considering the small angle assumption ($\cos\varphi^{wi} \approx 1$, and $\sin\varphi^{wi} \approx \varphi^{wi}$).

Defining a convenient wheelset *small-value* vertical coordinate $\bar{z}^{wi} = z^{wi} - r_0$, Eq. 8 can be written in matrix form as:

$$\begin{bmatrix} 0 & r_0 + f^{lk} & 1 & 0 \\ 1 & L^w & \varphi^{wi} & 0 \\ 0 & r_0 + f^{rk} & 0 & 1 \\ 1 & -L^w & 0 & \varphi^{wi} \end{bmatrix} \begin{bmatrix} \bar{z}^{wi} \\ \varphi^{wi} \\ s^{lk} \\ s^{rk} \end{bmatrix} + \begin{bmatrix} y^{wi} - y^{lir} \\ -f^{lk} - z^{lir} \\ y^{wi} - y^{rir} \\ -f^{rk} - z^{rir} \end{bmatrix} = \mathbf{0} \tag{9}$$

Equation 9 is the simplified form of the KEC constraints whose solution is obtained under the assumption that the wheelset lateral coordinate y^{wi} is the independent coordinate and the remaining vertical $\bar{z}^{wi}$, roll φ^{wi}, and transverse wheel parameters s^{lk} and s^{rk}, the dependent ones. Also note that in Eq. 9, the terms of the 4×4 matrix are not constant and depend on the roll angle φ^{wi}.

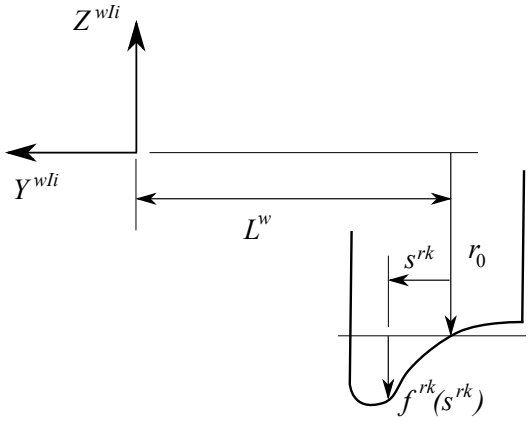

Figure 6: Right wheel equivalent KEC profile

3.3. Calculation of the KEC equivalent profiles

Figure 7 shows a comparison between a real (dashed dotted line) and equivalent (solid line) wheel profiles. Both profiles (that are used in the numerical examples of Sect. 7) produce the same wheelset-track relative kinematics.

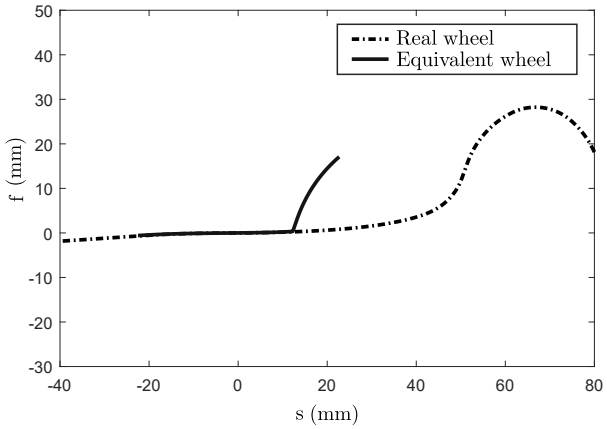

Figure 7: Real and equivalent wheel profiles comparison

The method used to find the KEC equivalent wheel profile requires first the analysis of the wheelset-track relative kinematics using the real profiles and zero irregularities. As a result, a contact lookup table is generated, which stores the motions $z^{wi} = z^{clt}(y^{wi})$ and $\varphi^{wi} = \varphi^{clt}(y^{wi})$ and the contact geometry parameters of the locations of the contact points as functions of discrete values of y^{wi}. The KEC equivalent wheel profiles are obtained solving Eq. 8 using the wheelset coordinates (y^{wi}, z^{wi} and φ^{wi}) as inputs, and the transverse equivalent wheel parameters and profile functions s^{lk}, s^{rk}, f^{lk} and f^{rk} shown in Fig. 6 as the outputs. The pairs $\left(s^{lk} - f^{lk}\right)$, $\left(s^{rk} - f^{rk}\right)$ constitute a tabulated version of the left and right KEC-equivalent profiles $f^{lk}(s^{lk})$ and $f^{rk}(s^{rk})$, respectively. Although the equivalent profiles are obtained using the contact solution for an ideal track without irregularities, its use in general tracks with irregularities is accurate, as demonstrated in [13].

3.4. Benefits of the KEC contact method

As explained in the previous Sect. 3.3, also for the KEC-method a lookup table has to be generated, as it is required for the analysis of the real profiles. This raises the question what the benefits of the KEC-method are. In this sense, the benefits can be listed as follows:

1. Modelling wheel-rail contact with lookup tables requires the use of the gauge irregularity as a second entry (the other entry is the wheelset lateral displacement y^{wi}). The amount of data to be stored and used for interpolation can be quite large. However, the CLT needed to find the KEC equivalent profiles has to be created just for an irregularity-free track (one single entry: y^{wi}). The resulting KEC-equivalent profiles are still approximately valid in the presence of irregularity. It has been shown [13] that the saving of computational time due to the reduced interpolations makes the KEC-method more efficient than the use of CLT while keeping a good accuracy.
2. The KEC-method allows the simulation of the 2-point contact scenarios without relying on an elastic contact in the flange (hybrid method). The use of two different approaches (constraint-based and elastic-based) to simulate the same phenomenon is a source of serious problems in railway simulations.

The rest of this paper explains how to deal with the 2-point contact scenario and the KEC-method.

4. Wheel-rail contact forces using the KEC-method

As the KEC-method is a constraint contact method, normal contact forces appear as a vector of generalized reaction forces into the equations of motion. However, for the computation of the tangential contact forces, several inputs such as creepages, surface curvatures and normal forces acting on the contact points are required. In this sense, when a KEC contact method is used, the values of these parameters may clearly differ from realistic values of real wheel-rail profiles because as presented in Sect. 3, the equivalence between KEC and real profiles is limited to the wheelset kinematic relation (z^{wi} and φ^{wi}). This implies that, for a proper analysis of the dynamic behaviour of a railway vehicle, contact forces should be applied at the real contact point locations in the real profiles instead of the equivalent ones.

The position (surface parameters) of the contact points in the real and equivalent profiles is calculated when obtaining the KEC-equivalent profiles. For each value of the wheelset lateral displacement, these surface parameters are stored as:

$$\begin{aligned} s^{lw} &= s^{lw}\left(s^{lk}\right), \quad s^{lr} = s^{lr}\left(s^{lk}\right) \\ s^{rw} &= s^{rw}\left(s^{rk}\right), \quad s^{rr} = s^{rr}\left(s^{rk}\right) \end{aligned} \tag{10}$$

being s^{lw} and s^{rw} the curve parameters of the left and right real wheels, and s^{lr} and s^{rr} the curve parameters of the left and right real rails.

4.1. KEC normal contact force

The components of the generalized reaction forces due to the constraints given in Eq. 9 associated with the wheelset vertical and roll-angle coordinates ($\bar{z}^{wi}$ and φ^{wi}) are the vertical force, Q_z^{reac}, and roll-torque, Q_φ^{reac}, acting on each wheelset due to the normal contact forces. Finding the normal contact forces in the real profiles from these reaction forces follows this procedure:

1. After the solution of the constraint equations of Eq. 9, lookup table functions of Eq. 10 are used to obtained the contact point curve parameters at the real profiles (s^{lw}, s^{rw}, s^{lr} and s^{rr}).
2. Normal directions of the left and right real rail contact points ($\mathbf{n}^{lr}$ and $\mathbf{n}^{rr}$) together with the local position vectors at the real wheels ($\mathbf{u}^{lw}$ and $\mathbf{u}^{rw}$) are obtained based on the calculated curve parameters.
3. Normal forces acting on the left and right wheels (F^{ln} and F^{rn} shown in Fig. 8) are calculated applying the following equilibrium of forces and moments:

$$\begin{aligned} Q_z^{reac} &= \left(F^{ln}\mathbf{n}^{lr} + F^{rn}\mathbf{n}^{rr}\right)\cdot\mathbf{k} \\ Q_\varphi^{reac} &= \left(\left(F^{ln}\mathbf{u}^{lw}\right)\times\mathbf{n}^{lr} + \left(F^{rn}\mathbf{u}^{rw}\right)\times\mathbf{n}^{rr}\right)\cdot\mathbf{i} \end{aligned} \tag{11}$$

being $\mathbf{i}$ and $\mathbf{k}$ the unit vectors along the longitudinal and vertical axes respectively. Equation 11 is a system of two linear equations with two unknowns: the normal contact forces acting on the real left and right wheels F^{ln} and F^{rn}, respectively.

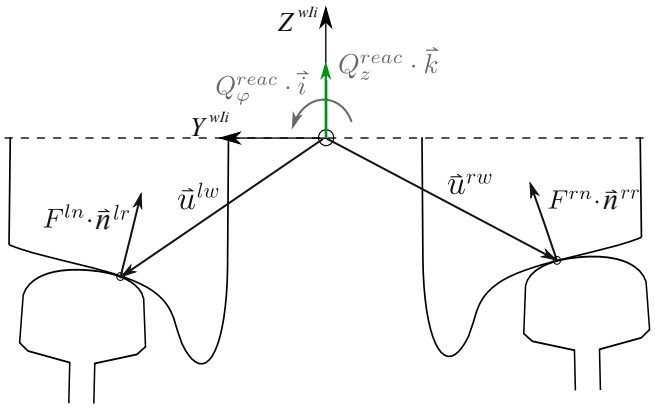

Figure 8: Computation of normal contact forces based on reaction forces

4.2. KEC tangential contact force

The computation of the creep forces using the KEC-method can be done using any of the common well-known tangential rolling-contact theories [1] (i.e. Kalker, Polach, etc.), since the required variables for its computation, such as the position of the contact points, their relative tangential velocities, normal forces and contact coefficients, are computed at the real wheel-rail profiles using the functions provided by Eq. 10 and the equilibrium of forces and moments of Eq. 11.

5. Two-point wheel-rail contact scenario using KEC-method

Two-point contact scenarios, which are crucial for the safety of the rolling stock, can be analysed using the KEC-method by softening contact constraints, as presented next.

5.1. Continuous piecewise linear approach for KEC constraints

One of the advantages of the KEC-method is the continuous evolution of the contact point in the equivalent wheel profile for every wheelset lateral position with respect to the track, while with real profiles, contact points follow finite jumps from tread to flange. Figure 9 shows the relation between the surface parameter s^{lk} in the equivalent left wheel profile and the surface parameter s^{lw} in the real left wheel profile (Eq. 10). It can be seen that for a certain value of the equivalent parameter s_f^{lk}, there are two simultaneous contact points in the real profile, s_f^{lw} and s_t^{lw}. This corresponds to a two-point wheel-rail contact scenario where at the left wheel one contact point is located at the flange, s_f^{lw}, and another one at the tread, s_t^{lw}.

From the mathematical point of view, the two-point contact shown in Fig. 9 is a discontinuity, which is generally problematic for numerical simulation; for the integration of a system of differential equations, this can lead to numerical instabilities. In order to avoid these instabilities, a regularization by a piecewise linear function shown as a solid blue line in Fig. 10 is proposed. This regularization function uses as parameters two short transition lengths $\Delta\bar{s}$ and $\Delta\hat{s}$. Regularized the discontinuity of the real-wheel surface parameter within the transition length $\Delta\bar{s}$, is equivalent to force a continuous transition from tread to flange in the wheel real profile along the *forbidden area*, while the length $\Delta\hat{s}$ allows a soft and continuous evolution of the contact point to the two-point scenario. In this sense, the forbidden area is defined by the segments of the wheel and rail profiles where the contact point can never be located due to incompatible curvatures. However, the normal contact force will not be applied there during the simulation, as shown in next section.

5.2. Normal and tangential contact forces in the two-point contact scenario

It is clear from the previous section that the use of the regularized contact KEC-constraints is computationally convenient, because it avoids finite jumps in the location of the contact force when moving from tread to flange. However, if contact forces are directly applied at the contact point in the forbidden area,

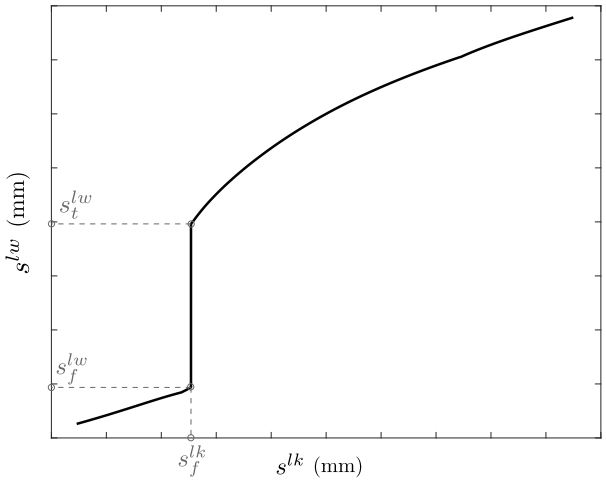

Figure 9: Transverse curve parameters relation between equivalent and real left wheel profiles

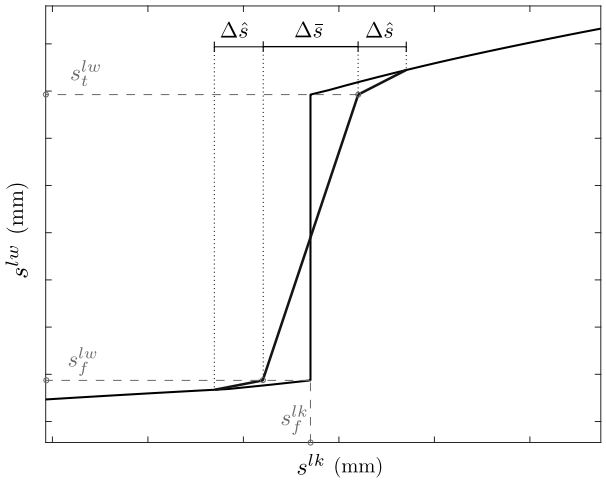

Figure 10: Linear regularization approach between equivalent and real curve profile parameters

the dynamic behaviour of a railway vehicle using this approach will not be accurate nor representative. Initially, during the transition of the contact point, the value of the normal contact force is obtained in the forbidden area by solving Eq. 11. In a second step, this force is transformed into two statically equivalent normal forces at the tread-end point (s_t^{lw}) and the flange-starting point (s_f^{lw}) as shown in Eq. 12. Static equivalence is guaranteed by the following equation:

$$F^n \cdot \mathbf{n}^r = F^f \cdot \mathbf{n}^f + F^t \cdot \mathbf{n}^t \tag{12}$$

where, as shown in Fig. 11, F^n and $\mathbf{n}^r$ are the normal force and normal direction in the forbidden area, while F^t, $\mathbf{n}^t$, F^f and $\mathbf{n}^f$ are the same at the tread-end point and the flange-starting point, respectively. In this equation, superscripts l and r for *left* and *right* contacts are omitted for simplicity. The y and z components of Eq. 12 constitute a linear system of two equations with two unknowns: the two normal contact forces F^f and F^t acting on the flange and tread respectively. The resulting forces are such that the force on the flange increases smoothly from zero, and the tread force decreases smoothly, as the contact force on the forbidden area moves continuously from tread to flange.

It can be observed that the procedure presented to account for two-point normal contact forces acting

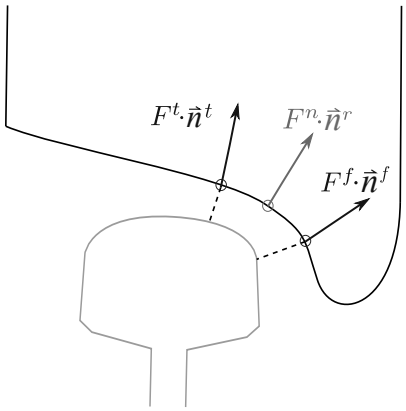

Figure 11: Two-point wheel-rail normal contact force computation

on the wheel tread and flange by Eq. 12 does not account for the moment-balance due to the forces F^n, F^f and F^t. In other words, the two forces F^f and F^t are not fully equivalent to F^n. However, because the distance between tread and flange is very small compared to the wheelset half-width (approximate distance used to compute the torque), the difference of the torque due to F^f and F^t and the torque due to F^n is very small. As it will be shown in Sect. 7 with simulation results, the error produced is marginal.

Finally, tangential contact forces can be computed using, as inputs, the already obtained normal contact forces and directions at the tread-end point and the flange-starting point.

6. Dynamics equations of motion

The dynamic equations of motion of railway vehicles subject to contact constraints can be systematically derived based on the well-known Newton-Euler equations of vehicle bodies. These equations can be written in compact form as:

$$\begin{aligned} \mathbf{M}\ddot{\mathbf{q}} + \mathbf{C}_{\mathbf{q}}^T \lambda &= \mathbf{Q} \\ \mathbf{C}\left(\mathbf{q}\right) &= \mathbf{0} \end{aligned} \tag{13}$$

where $\mathbf{M}$ is the generalized mass matrix, $\mathbf{q}$ is the vector of generalized coordinates, $\mathbf{C}$ is the vector of constraints (KEC contact constraints), $\mathbf{C_q}$ is the Jacobian of these constraints, λ is the vector of Lagrange multipliers and $\mathbf{Q}$ is the vector of generalized forces that includes, among others, the tangential contact forces.

Recall that in Eq. 13, the term $\mathbf{C}_{\mathbf{q}}^T \lambda$ includes the reaction generalized forces associated with contact constraints. These are the generalized normal contact forces that enter into the equations of motion and are needed to compute creep forces. However, because Eq. 13 is a system of differential algebraic equations, normal contact forces used to compute tangential forces are extracted from the previous time step. In addition, note that the procedure presented in Sect. 5 to transform these normal reaction forces into normal ones acting on the contact points is only derived to serve as inputs for the calculation of the tangential forces that appear in $\mathbf{Q}$.

7. Numerical examples

This section presents simulation results of two different case studies; (1) a single wheelset negotiating a small-radius curve using the proposed KEC approach and (2) a three-body suspended vehicle formed by two wheelsets and a bogie frame negotiating a large radius curve using the proposed approach and the well-known fully 3D elastic contact approach [3]. For both case studies, Polach tangential rolling contact theory [26] is used. The purpose of the first case study is to analyse a clear two-point wheel-rail contact scenario with the proposed KEC method. Because the dynamics of an unsuspended wheelset is well known,

this example is ideal to show the output of the modelling of the two-point contact scenario while avoiding the influence of other bodies or suspension elements. The second case study seeks to validate and compare the proposed approach with respect to the classical 3D elastic contact approach in terms of accuracy and computational efficiency. To that end, a bogie vehicle negotiating a larger radius curve than the first case study is analysed to experience a situation in which only the leading wheelset experiences two-point contacts allowing the rear one to adopt its stationary curve position due to suspension.

This section is divided as follows: Sects. 7.1 and 7.2 present the features and simulation results of the first case study and Sects. 7.3 and 7.4 present the same for the second one respectively. Finally, Sect. 7.5 provides the computational comparison of the bogie case study using the proposed KEC method and the 3D elastic contact one.

7.1. Single wheelset case study features

The proposed first case study is a single wheelset (m = 1109 kg, $I_x = I_z$ = 605.9 kg·m^2 and I_y = 61.6 kg·m^2) negotiating, at a constant forward velocity of V = 10 m/s, a 1435 mm gauge track without irregularities formed by the following three segments: 20-m tangent, 10-m transition and 300-m left curve of R = 100 m radius segment without superelevation. Wheel and rail profiles shown in Fig. 12 are the standard S1002 for the wheels whose nominal radius is r_0 = 0.46 m and the LB.140-AREA profile for the rails (140 lb/yd standardized by the American Railway Engineering Association, AREA). In addition, rails are inclined an angle 1/40.

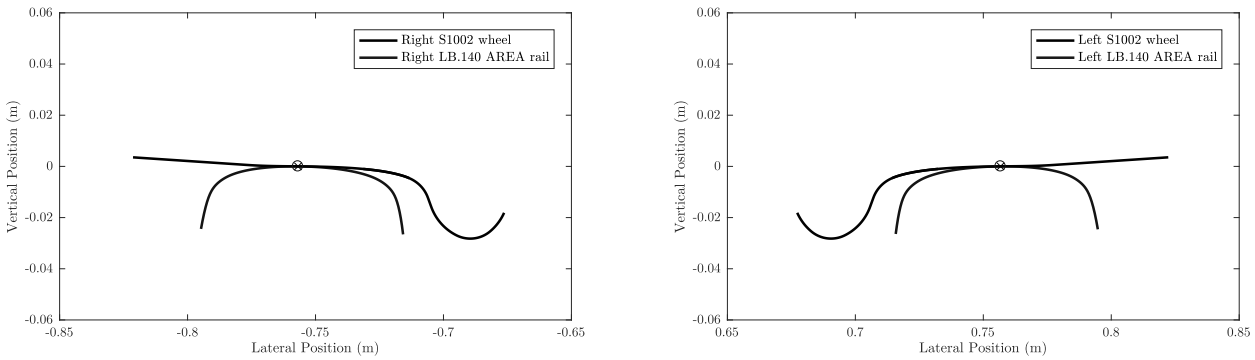

Figure 12: Real wheel-rail profile combination

Wheelset relative track kinematics using these profiles (vertical and roll angle coordinates) are shown in Fig. 13, which are used as inputs for the computation of the equivalent wheel profile as shown in Sect. 3.3. Based on Fig. 13, the real S1002 wheel and LB.140-AREA rail profiles combination gives a clear contact point jump from tread to flange at a lateral wheelset displacement of ±12.30 mm, which makes it ideal to analyse the capability of the proposed contact approach. In addition, the equivalent wheel profile obtained considering this kinematics is the one previously shown in Fig. 7.

The continuous piecewise linear approach to smooth the KEC constraints presented in Sect. 5.1 is applied using the values given in Table. 2 for the parameters. In Fig. 14, the regularized relation of the kinematics between the equivalent and real wheel profiles is drawn as a solid blue line, while the original non-regularized relation is drawn as a black dashed line. Based on the parameters of Table 2, the position in which the first two-point contact scenario occurs is predicted numerically 1 mm of wheel transverse parameter before its real wheel position.

7.2. Unsuspended wheelset simulation results

First, the motions of the wheelset negotiating the small-radius (R = 100 m) curved track are considered. Figure 15 shows its lateral displacement with respect to the track and Fig. 16 shows its vertical coordinate with respect to the reference position.

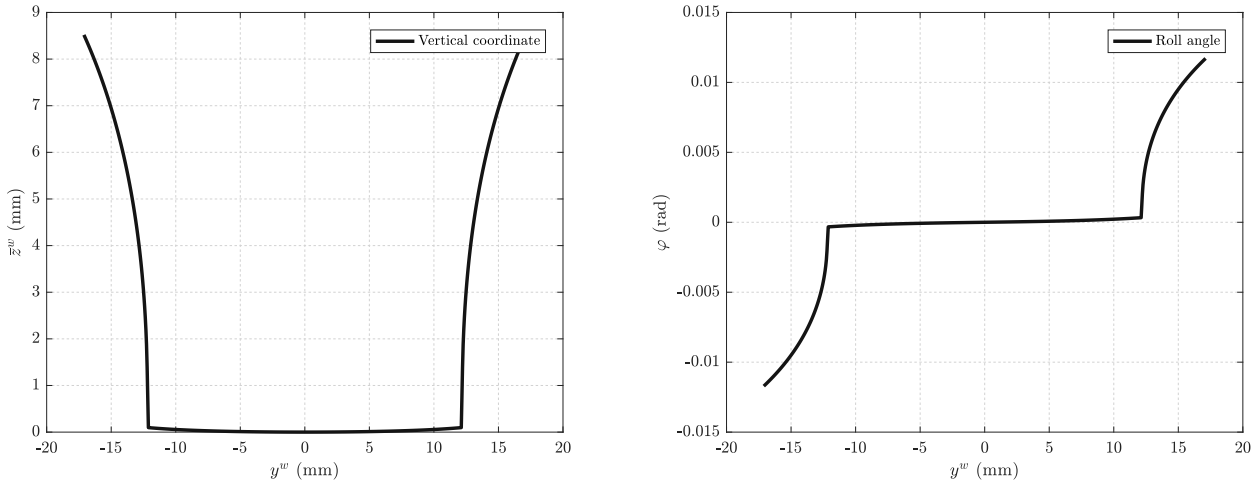

Figure 13: Wheelset relative track kinematics

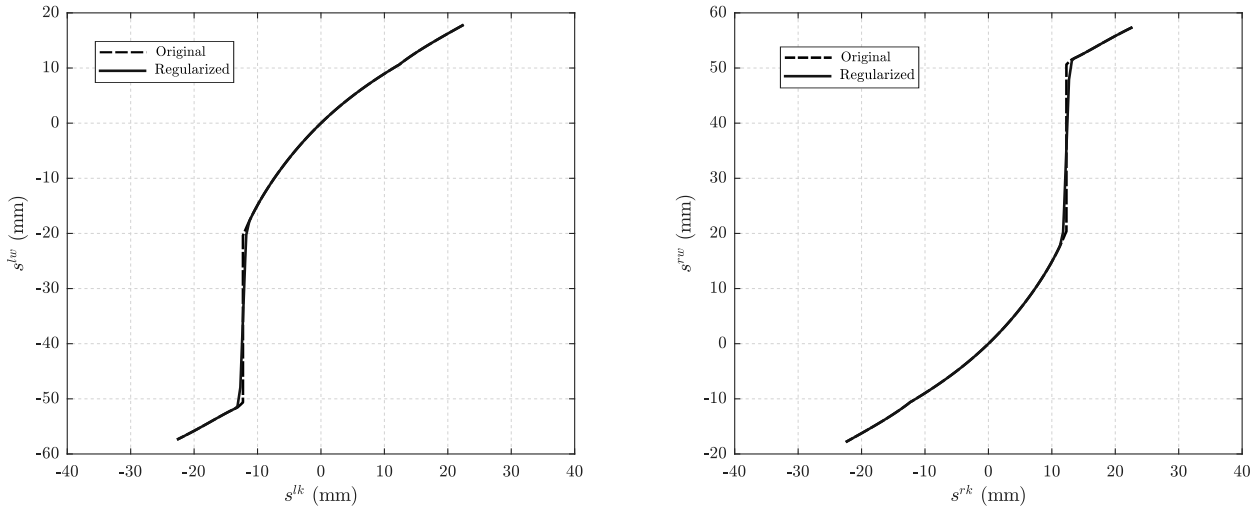

Figure 14: Curve parameter relation for the left and right equivalent and real wheels when KEC constraints in the vicinity of the two-point wheel-rail contact scenario are regularized.

It can be observed at Fig. 15 that the wheelset enters the transition curve at 20 m distance reaching the flange clearance at 30 m distance. From this point on and due to the wheelset inertia, some consecutive two-point wheel-rail contact situations occur until the wheelset reaches the stationary position at the two-point contact scenario. Because it is a left curve, the two-point continuous contact at 10 m/s forward velocity and 100-m radius curve happens at $y^w = -12.13$ mm.

The wheelset vertical displacement with respect to the reference position of Fig. 16 shows that the wheelset tends to climb several times before it reaches the stationary position. This happens when the first two-point contact scenario appears when the wheelset leaves the tangent track segment and enters the curved one. However, this behaviour is expected due to the features of the case study: a single wheelset body without suspension elements that negotiates a small radius curve at a relatively moderate velocity. Even in such an highly dynamic process for a constraint contact like the KEC-method, the proposed approach deals efficiently with it. The constant two-point contact scenario for this study gives a wheelset relative vertical displacement of $\bar{z}^w = 0.22$ mm.

To show the calculated contact point positions at the wheel, Fig. 17 compares their locations solving the

Table 2: Transverse curve parameters for the piecewise linear regularization of KEC constraints at the left two-point contact scenario. Symmetric values at s are obtained for the right two-point contact scenario

$\Delta\bar{s}$	1.00 mm	Transition length at the *forbidden* area
$\Delta\hat{s}$	0.50 mm	Transition length to reach the *forbidden* area
s_f^{lk}	-12.30 mm	Flange contact at equivalent wheel profile
s_f^{lw}	-50.64 mm	Flange contact at real wheel profile
s_t^{lw}	-20.37 mm	Tread contact at real wheel profile

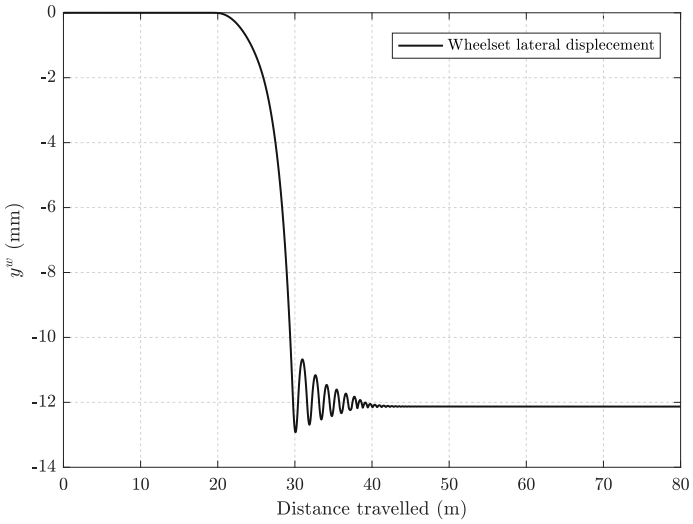

Figure 15: Wheelset lateral displacement with respect to the track centreline

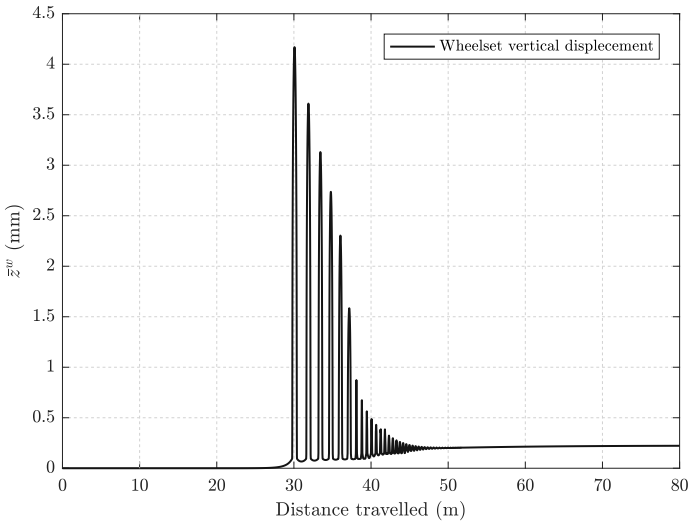

Figure 16: Wheelset relative vertical displacement with respect to the reference position

linear regularization approach with their real locations considering the finite contact point jump between

tread and flange. As it is shown, softening the constraint equations provides unrealistic contact points between tread and flange drawn as blue crosses. However, in computational terms, this computation is quite effortless and efficient. The transformation of the fictitious contact point locations into real contact point ones by using Eq. 10 is drawn in green circles. These are the exact locations where the tangential contact forces are calculated: factual tread and flange positions.

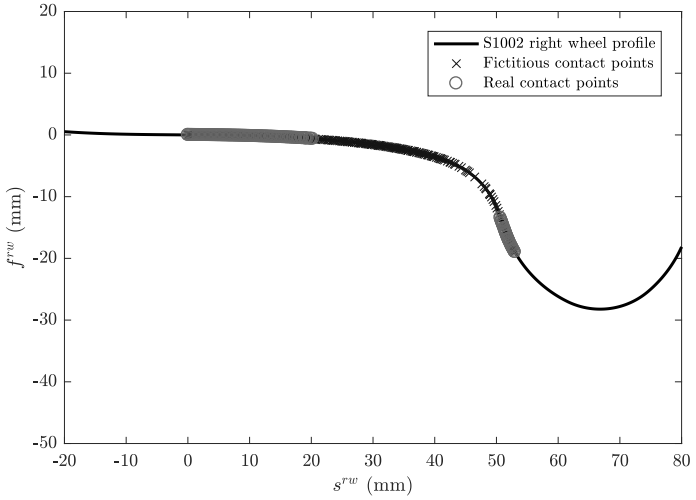

Figure 17: Contact point positions at the right S1002 wheel for regularized KEC constraints (blue crosses) and equivalent real contact point positions (green circles).

Additionally, normal contact forces obtained after the transformation of the generalized reaction forces into forces acting on the real contact points are shown in Fig. 18 for the right wheel, where two-point contact occurs. In dashed dark line, the resultant normal force F^n acting on the wheel when considering the KEC constraints, is plotted. This force can be applied at a real or fictitious contact point depending on the solution of the KEC constraints. Also, in blue and green line, the normal forces acting on the tread and flange F^t and F^f obtained by the use of the continuous regularized approach transformation of Eq. 12 are drawn. It can be seen that, when the wheelset runs the tangent track segment, the resultant normal force acting on the wheel F^n is the same as the one acting on the tread F^t since there is not a two-point contact scenario. However, when the wheelset negotiates the curve, the resultant normal force is acting on the forbidden area and it is consequently distributed to the tread and flange by means of Eq. 12. This is clearly seen when the wheelset reaches its constant position to negotiate the curve: the two-point constant contact scenario gives the following scalar normal forces: $F^t = 4.96$ kN at the tread, $F^f = 0.96$ kN at the flange and $F^n = 5.41$ kN as the resultant of the reaction forces at the right wheel.

Lastly, as presented in Sect. 5.2, the normal force transformation of Eq. 12 neglects the equilibrium of moments produced by the transformed forces. For this reason, Fig. 19 shows the comparison between the torque obtained as a reaction force and the resultant torque produced by the transformed normal forces. It can be seen that the error produced when a two-point contact scenario occurs is quite low. When the wheelset reaches its constant position at the curve, the relative error produced at the torque is 6.55%. Recall that the torque obtained as a reaction force is the one that enters into the equations of motion while the torque that the transformed normal forces produce, is not considered. Only the forces that produce such moment are the inputs for the computation of the tangential contact. Thus, neglecting the equilibrium of moments in this transformation can be considered as a reasonable assumption.

7.3. Bogie vehicle case study features

The proposed second case study is a bogie vehicle formed by two wheelsets similar to the one used at Sect. 7.1 and a bogie frame ($m_{bg} = 1500$ kg, $I_x = 1200$ kg·m^2, $I_y = 2400$ kg·m^2 and $I_z = 1500$ kg·m^2) with four simple vertical spring-damper elements as primary suspension whose stiffnesses and damping coefficients

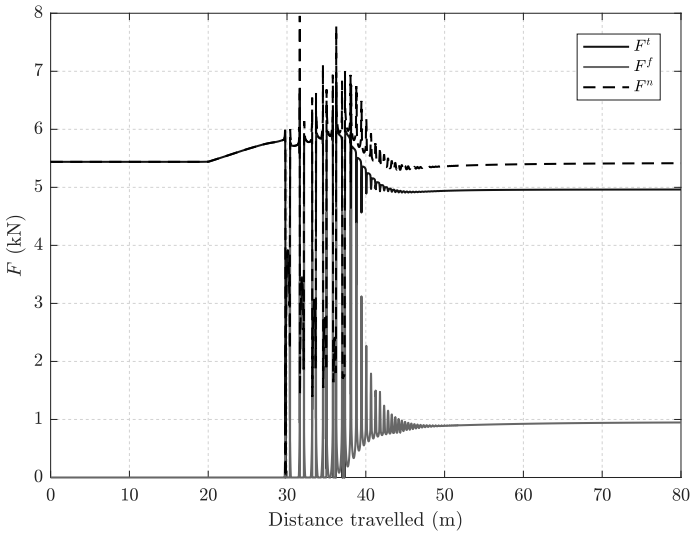

Figure 18: Right wheel normal contact forces used as inputs for the computation of tangential contact.

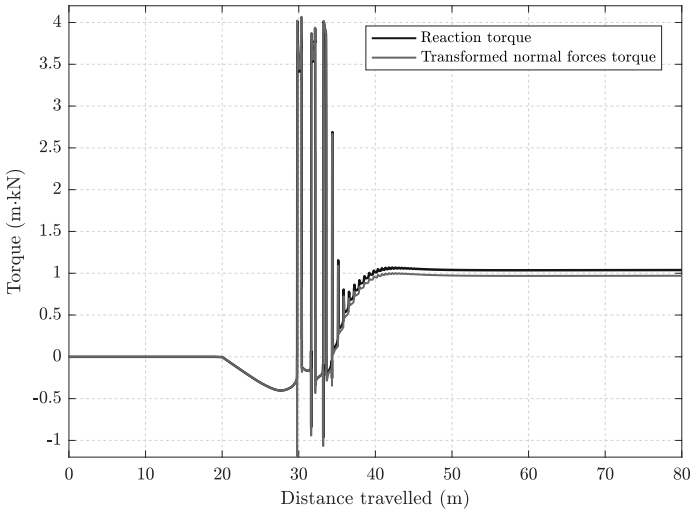

Figure 19: Comparison between the torque produced by the constraint reaction forces and by the transformed normal contact forces of the continuous regularization approach.

to axial and shear deformations are $k_{susp} = 2.0 \cdot 10^6$ N/m, $k_{susp}^{shear} = 1.8 \cdot 10^6$ N/m, $c_{susp} = 6 \cdot 10^4$ N·s/m and $c_{susp}^{shear} = 5 \cdot 10^4$ N·s/m, respectively. The vehicle negotiates, at a constant forward velocity of $V = 10$ m/s, a similar ideal track than in Sect. 7.1 but considering a curved segment with radius $R = 1000$ m for the purpose of experiencing two-point wheel-rail contact scenarios only at the leading wheelset.

Parameters used for the numerical results using the KEC approach are the same given in Table 2. In addition, as the 3D elastic contact approach used to compare with the proposed KEC method considers a compliant force at the contact points, two different Hertzian stiffnesses and damping coefficients shown in Table 3 are used to evaluate their influence in the numerical results. In this context, the compliant force model F used for the elastic approach is given as follows [3]:

$$F = k_h \delta^{3/2} + c_h \dot{\delta} |\delta| \tag{14}$$

where k_h and c_h are the Hertzian constant stiffness and damping coefficients, and δ and $\dot{\delta}$ the surfaces

Table 3: Hertzian parameters used for the 3D elastic contact approach

Elastic model type 1	$k_h = 1 \cdot 10^{10}$ N/m$^{3/2}$ $c_h = 1 \cdot 10^{7}$ N·s/m^2
Elastic model type 2	$k_h = 1 \cdot 10^{12}$ N/m$^{3/2}$ $c_h = 1 \cdot 10^{7}$ N·s/m^2

indentation and indentation rate respectively. Note that values given for k_h pretend to consider the effect of the structural stiffness of the wheel combined with the elastic half-space assumption of the solids in contact.

7.4. Bogie vehicle simulation results

The kinematic comparison of the bogie vehicle is presented in Figs. 20, 21 and 22. Figure 20 shows the wheelsets and bogie frame lateral displacements with respect to time as the vehicle negotiates the track when the proposed KEC approach (left figure) and the two elastic models (centre and right figure) are considered. It can be seen that the three approaches reproduce the two-point contact scenario only at the front wheelset while the rear one adopts a stationary position at the curve. Using the KEC method with the regularized transition approach (left figure), clean values of the vehicle lateral displacements are obtained. Similarly, when analysing the results given by the elastic approaches, clean values can be observed when the Hertzian parameters of the elastic type 1 are used (centre figure) but noisy values appear when the elastic type 2 is used (right figure). This is reasonable since the elastic type 2 considers a Hertzian stiffness $k_h = 1 \cdot 10^{12}$ N/m$^{3/2}$, which is 100 times higher than the one used at the elastic type 1. However, based on the surfaces curvatures at the flange contact [25], the Hertzian stiffness of the elastic type 2 is relatively more realistic than the elastic type 1.

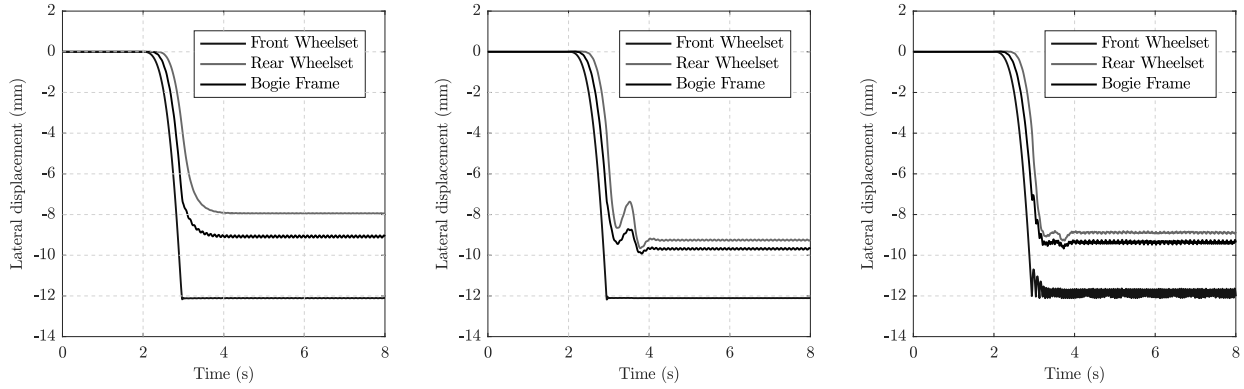

Figure 20: Comparison between the lateral displacements obtained at the bogie vehicle. (Left): proposed KEC approach. (Centre): elastic approach type 1. (Right): elastic approach type 2.

Figure 21 shows a similar comparison for the vehicles yaw angles using the three different approaches. In here, the same conclusions can be extracted as in Fig. 20. Both KEC and the elastic approaches reproduce a similar behaviour of the vehicles yaw angles, being the stiffer elastic approach (type 2) the one that results in a higher frequency content solution.

To check the differences in the evaluation of the two-point contact scenario, Fig. 22 shows a direct comparison for the leading wheelset using the KEC and the elastic contact approaches. The comparison is done for the wheelset lateral displacement (left figure) and for the yaw angle (right figure). In addition, the stationary positions of the vehicle bodies at the curve are given in Table 4. It can be seen that the accuracy of the results given by the proposed KEC method for the evaluation of the two-point contact scenario is adequate and of the same order of magnitude than the elastic approach.

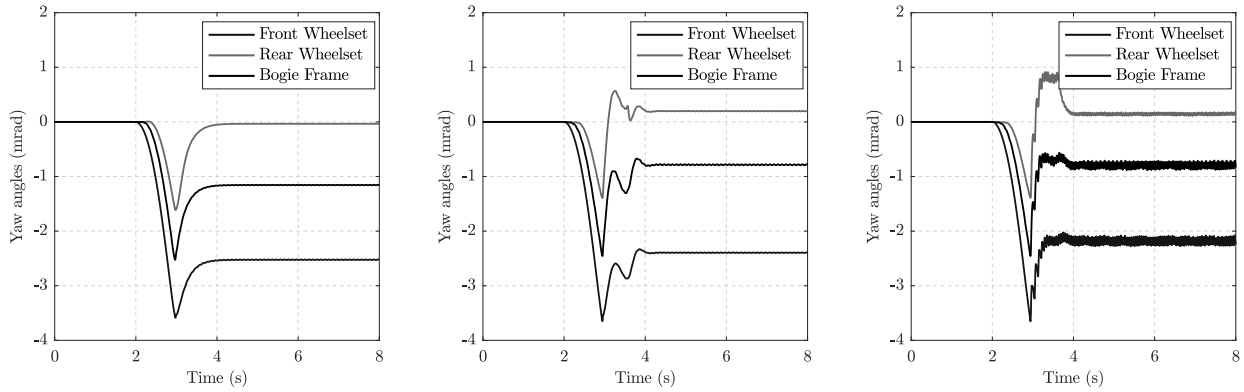

Figure 21: Comparison between the yaw angles obtained at the bogie vehicle. (Left): proposed KEC approach. (Centre): elastic approach type 1. (Right): elastic approach type 2.

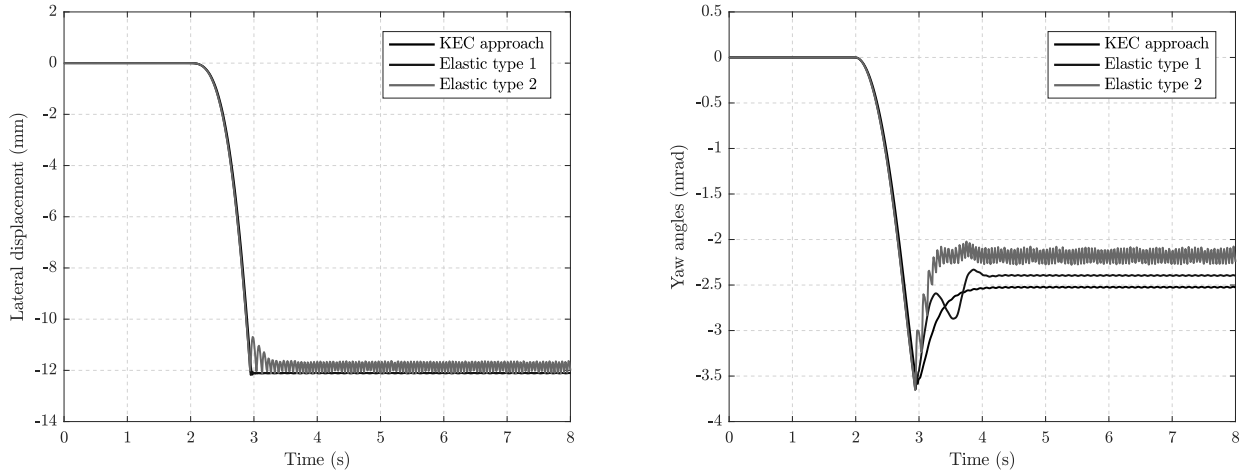

Figure 22: Leading wheelset kinematic comparison using KEC and Elastic type 1 and 2 approaches. (Left): wheelset lateral displacement. (Right): wheelset yaw angle.

Table 4: Bodies stationary positions at the curve.

		Lateral displacement y (mm)	*Yaw* angle ψ (mrad)
Front Wheelset	KEC	-12.11	-2.525
	Elastic-1	-12.11	-2.395
	Elastic-2	-11.85	-2.230
Rear Wheelset	KEC	-7.94	-0.035
	Elastic-1	-9.26	0.195
	Elastic-2	-8.91	0.135
Bogie Frame	KEC	-9.08	-1.155
	Elastic-1	-9.69	-0.785
	Elastic-2	-9.35	-0.810

7.5. Computational efficiency

Finally, to analyse the computational efficiency of the proposed KEC method, computing times of the bogie vehicle case study are presented in this section. The simulations have been performed using an in-house computer code developed in Matlab R2016b with a computer with processor Intel Core i7-7700K @ 4.20 GHz. The code is not optimized for computational efficiency so function parallelization or *Mex functions* written in C or Fortran are not used. The different approaches are integrated numerically forward in time using the adaptable time step *ode15s* Matlab integrator considering default parameters and a maximum time step of $5 \cdot 10^{-4}$ s. Also, contact constraints are solved using the well-known Newton-Rhapson algorithm.

Table 5 summarises the computational cost of the bogie vehicle simulations given in Sect. 7.4. The 8-s vehicle simulation using the proposed KEC method takes a total simulation time of 73.7 s while the elastic approach with the Hertzian parameters type 1 and 2 takes 1033.3 and 927.1 s respectively. This means that the proposed approach is 12.6 times more efficient than the fastest 3D elastic contact simulation. One of the reasons that justifies such difference is the number of function evaluations of the contact constraints. Due to the simplicity and assumptions adopted for the KEC constraints (simplified planar contact), they are evaluated almost once per time step, essentially as if they were a system of linear algebraic equations. However, the 3D elastic contact constraints require a considerably higher number of function evaluations in the Newton-Rhapson algorithm, as it can be seen in Table 5. Therefore, the great computational efficiency of the proposed KEC method is clearly proven.

Table 5: Computational cost at the bogie vehicle 8-seconds simulation case study.

	KEC	Elastic-1	Elastic-2	Ratio Elastic/KEC
Total simulation time	73.7 s	1033.3 s	927.1 s	12.6
Number of contact constraints evaluations	$7.37 \cdot 10^4$	$1.973 \cdot 10^6$	$1.708 \cdot 10^6$	23.2

8. Summary and conclusions

In this work, a continuous analysis of the two-point wheel-rail contact scenario using contact constraints is proposed. The work is based on the *Knife-edge Equivalent Contact method* (KEC-method), in which an equivalent wheel profile contacts a single-point rail producing the same wheelset relative track kinematics as using real profiles. The features of the KEC constraints allow a regularization of the constraints in the vicinity of a two-point contact scenario by defining a piecewise linear relation between the locations of the contact points on the equivalent and real profiles. The proposed approach avoids the discontinuity problems in numerical simulations associated with the wheel-rail separation common in two-point contact scenarios since the contact point moves continuously from tread to flange avoiding jumps. However, this smoothed transition provides contact points that act on fictitious locations of the wheel between tread and flange. For this reason, in order to account for tangential contact, those normal forces that act on fictitious locations are transformed into normal ones acting on real locations of the wheel tread and flange by maintaining the equilibrium of forces at the wheel. This way, the transformed normal forces are then used as inputs for the computation of friction.

Comparing the use of KEC method to lookup tables, the latter is clearly simpler in pre-processing stage. This comparison is clear since the KEC method starts with the calculation of the lookup tables and it requires a few more calculations. Even in the processing stage, the KEC method is, in general, more sophisticated than the use of lookup tables. However, the more involved calculations of the KEC method are compensated by the possibility to simulate two-point contact scenarios with constraints and wheel climb.

The proposed approach is applied to two different case studies. First, a single wheelset running a small radius curve ($R = 100$ m) at a relatively moderate forward velocity ($V = 10$ m/s) to experience two-point

contact scenarios. After a preprocessing stage in which the equivalent profile is calculated, results show that the two-point contact scenario using constraints can be easily evaluated providing clean values of wheelset coordinates and reasonable contact forces. The second case study analyses a wheelset body negotiating a curve ($R = 1000$ m) at $V = 10$ m/s. Because the curve radius is larger than the first case study, only the leading wheelset of the vehicle experiences a two-point wheel rail contact, while the rear one and bogie frame adopt a stationary position at the curve. This second case study is compared to the results given by the fully 3D elastic contact method using two different sets of Hertzian parameters. The kinematic comparison shows that both approaches result in a similar dynamic behaviour of the vehicle bodies while the computational efficiency of the proposed KEC approach is greatly better than in the elastic contact one.

Acknowledgements

This work is supported by the Spanish Ministry of Science, Innovation and Universities under Project Reference TRA2017-86355-C2-1-R. This support is gratefully acknowledged.

Conflicts of interest

The authors declare that there is no conflict of interest to this work.

References

References

[1] S. Z. Meymand, A. Keylin, M. Ahmadian, A survey of wheel–rail contact models for rail vehicles, Vehicle System Dynamics 54 (3) (2016) 386–428. doi:10.1080/00423114.2015.1137956.

[2] A. A. Shabana, M. Tobaa, H. Sugiyama, K. E. Zaazaa, On the computer formulations of the wheel/rail contact problem, Nonlinear Dynamics 40 (2) (2005) 169–193. doi:10.1007/s11071-005-5200-y.

[3] A. A. Shabana, K. E. Zaazaa, J. L. Escalona, J. R. Sany, Development of elastic force model for wheel/rail contact problems, Journal of sound and vibration 269 (1-2) (2004) 295–325. doi:10.1016/S0022-460X(03)00074-9.

[4] H. Magalhães, F. Marques, B. Liu, P. Antunes, J. Pombo, P. Flores, J. Ambrósio, J. Piotrowski, S. Bruni, Implementation of a non-hertzian contact model for railway dynamic application, Multibody System Dynamics (2019) 1–38doi:10.1007/s11044-019-09688-y.

[5] J. Pombo, J. Ambrósio, M. Silva, A new wheel–rail contact model for railway dynamics, Vehicle System Dynamics 45 (2) (2007) 165–189. doi:10.1080/00423110600996017.

[6] J. C. Pombo, J. A. Ambrósio, Application of a wheel–rail contact model to railway dynamics in small radius curved tracks, Multibody System Dynamics 19 (1-2) (2008) 91–114. doi:10.1007/s11044-007-9094-y.

[7] J. Pombo, J. Ambrósio, An alternative method to include track irregularities in railway vehicle dynamic analyses, Nonlinear Dynamics 68 (1-2) (2012) 161–176. doi:10.1007/s11071-011-0212-2.

[8] P. Antunes, H. Magalhães, J. Ambrósio, J. Pombo, J. Costa, A co-simulation approach to the wheel–rail contact with flexible railway track, Multibody System Dynamics 45 (2) (2019) 245–272. doi:10.1007/s11044-018-09646-0.

[9] M. Malvezzi, E. Meli, S. Falomi, A. Rindi, Determination of wheel–rail contact points with semianalytic methods, Multibody System Dynamics 20 (4) (2008) 327–358. doi:10.1007/s11044-008-9123-5.

[10] S. Falomi, M. Malvezzi, E. Meli, Multibody modeling of railway vehicles: innovative algorithms for the detection of wheel–rail contact points, Wear 271 (1-2) (2011) 453–461. doi:10.1016/j.wear.2010.10.039.

[11] L. Baeza, D. J. Thompson, G. Squicciarini, F. D. Denia, Method for obtaining the wheel–rail contact location and its application to the normal problem calculation through 'contact', Vehicle System Dynamics (2018) 1–13doi:10.1080/00423114.2018.1439178.

[12] S. Muñoz, J. F. Aceituno, P. Urda, J. L. Escalona, Multibody model of railway vehicles with weakly coupled vertical and lateral dynamics, Mechanical Systems and Signal Processing 115 (2019) 570–592. doi:10.1016/j.ymssp.2018.06.019.

[13] J. L. Escalona, J. F. Aceituno, P. Urda, O. Balling, Railroad multibody simulation with the knife-edge-equivalent wheel-rail constraint equations, Multibody System Dynamics (2019). doi:10.1007/s11044-019-09708-x.

[14] J. L. Escalona, J. F. Aceituno, Multibody simulation of railway vehicles with contact lookup tables, International Journal of Mechanical Sciences 155 (2019) 571 – 582. doi:https://doi.org/10.1016/j.ijmecsci.2018.01.020.

[15] J. Santamaría, E. Vadillo, J. Gómez, A comprehensive method for the elastic calculation of the two-point wheel–rail contact, Vehicle System Dynamics 44 (sup1) (2006) 240–250. doi:10.1080/00423110600870337.

[16] H. Sugiyama, K. Araki, Y. Suda, On-line and off-line wheel/rail contact algorithm in the analysis of multibody railroad vehicle systems, Journal of mechanical science and technology 23 (4) (2009) 991–996. doi:10.1007/s12206-009-0327-2.

[17] H. Sugiyama, T. Sekiguchi, R. Matsumura, S. Yamashita, Y. Suda, Wheel/rail contact dynamics in turnout negotiations with combined nodal and non-conformal contact approach, Multibody System Dynamics 27 (1) (2012) 55–74. doi:10.1007/s11044-011-9252-0.

[18] J. Piotrowski, B. Liu, S. Bruni, The kalker book of tables for non-hertzian contact of wheel and rail, Vehicle System Dynamics 55 (6) (2017) 875–901. doi:10.1080/00423114.2017.1291980.

[19] F. Marques, H. Magalhães, B. Liu, J. Pombo, P. Flores, J. Ambrósio, J. Piotrowski, S. Bruni, On the generation of enhanced lookup tables for wheel-rail contact models, Wear 434 (2019) 202993. doi:https://doi.org/10.1016/j.wear.2019.202993.

[20] J. Piotrowski, S. Bruni, B. Liu, E. Di Gialleonardo, A fast method for determination of creep forces in non-hertzian contact of wheel and rail based on a book of tables, Multibody System Dynamics 45 (2) (2019) 169–184. doi:10.1007/s11044-018-09635-3.

[21] G. Schupp, C. Weidemann, L. Mauer, Modelling the contact between wheel and rail within multibody system simulation, Vehicle System Dynamics 41 (5) (2004) 349–364. doi:10.1080/00423110412331300326.

[22] H. Netter, G. Schupp, W. Rulka, K. Schroeder, New aspects of contact modelling and validation within multibody system simulation of railway vehicles, Vehicle System Dynamics 29 (S1) (1998) 246–269. doi:10.1080/00423119808969563.

[23] W. Rulka, A. Eichberger, Simpack an analysis and design tool for mechanical systems, Vehicle system dynamics 22 (S1) (1993) 122–126. doi:10.1080/00423119308969483.

[24] J. L. Escalona, J. Valverde, J. Mayo, J. Domínguez, Reference motion in deformable bodies under rigid body motion and vibration. part ii: evaluation of the coefficient of restitution for impacts, Journal of Sound and Vibration 264 (2003) 1057–1072. doi:10.1016/S0022-460X(02)01188-4.

[25] A. A. Shabana, K. E. Zaazaa, H. Sugiyama, Railroad vehicle dynamics: a computational approach, CRC press, 2007. doi:10.1201/9781420045857.

[26] O. Polach, A fast wheel-rail forces calculation computer code, Vehicle System Dynamics 33 (sup1) (1999) 728–739. doi:10.1080/00423114.1999.12063125.